ELSEVIER

Journal of Nuclear Materials 251 (1997) 200–217

journal of nuclear materials

Defect production in ceramics

S.J. Zinkle [a,*], C. Kinoshita [b]

[a] *Metals and Ceramics Division, Oak Ridge National Laboratory, PO Box 2008, Oak Ridge, TN 37831-6376, USA*
[b] *Department of Nuclear Engineering, Kyushu University 36, Hakozaki, Fukuoka 812, Japan*

Abstract

A review is given of several important defect production and accumulation parameters for irradiated ceramics. Materials covered in this review include alumina, magnesia, spinel, silicon carbide, silicon nitride, aluminum nitride and diamond. Whereas threshold displacement energies for many ceramics are known within a reasonable level of uncertainty (with notable exceptions being AlN and Si_3N_4), relatively little information exists on the equally important parameters of surviving defect fraction (defect production efficiency) and point defect migration energies for most ceramics. Very little fundamental displacement damage information is available for nitride ceramics. The role of subthreshold irradiation on defect migration and microstructural evolution is also briefly discussed. © 1997 Elsevier Science B.V.

1. Introduction

Radiation effects in ceramics have been studied for many years, with the most intense period of research occurring in the 1960s and 1970s. A sound understanding of radiation effects in ceramics is desired due to the importance of these materials in electronic applications (ion beam processing, high temperature semiconductors in radiation environments, etc.), fission reactor fuel burnup and reconstitution, nuclear waste disposal, and advanced energy concepts such as fusion energy and nuclear thermionic systems. Several factors cause radiation effects in ceramics to be more complex than in metals. Ceramics generally consist of multiple sublattices, each with different atomic masses and displacement energies. In addition, ionizing radiation can affect defect production [1] and/or migration [2] in many ceramics. As a consequence of this complexity, many of the fundamental aspects of radiation effects are not as well understood for ceramics compared to metals.

A multitude of experimental techniques are available for studying radiation effects in ceramics. These techniques include optical spectroscopy (absorption, luminescence, radio-luminescence, etc.), electron paramagnetic resonance (EPR), thermally stimulated spectroscopy (luminescence, electrical conductivity), positron annihilation, lattice parameter and length change measurements. Techniques such as optical spectroscopy and EPR are particularly valuable since they can provide information about a specific type of point defect, including its charge state (e.g., an F^+ center, an oxygen vacancy with a single trapped electron). Such defect-specific probes are generally not available for radiation effects studies in metals. However, detailed and time-consuming studies are required in order to determine the identity of the defect responsible for a particular EPR or optical signal. Consequently, only a relatively small proportion of the numerous point defect states that occur in different ceramics have been uniquely identified by these techniques.

Numerous reviews on radiation effects in ceramics have been published [1,3–8]. The objective of this paper is to review the available information on several key fundamental parameters that describe defect production and migration in irradiated ceramics. Specifically, this review will focus on the experimental and calculated values of threshold displacement energies for several technologically important oxide and carbide ceramics. Available information on the mobility of point defects and the defect production efficiency will also be reviewed, including the role of ionizing (non-displacive) radiation on defect migration. One well-studied topic which will not be addressed in this review is defect production by ionizing radiation. This

* Corresponding author. Tel.: +1-423 576 7220; fax: +1-423 574 0641; e-mail: zinklesj@ornl.gov.

PII S0022-3115(97)00224-9

defect production mechanism is very important in certain ceramic systems such as alkali halides and silica [1,3,8,9], but produces negligible amounts of displacement damage compared to elastic collisions in the ceramics covered in this review: Al_2O_3, MgO, $MgAl_2O_4$, CaO, ZnO, UO_2, BeO, diamond, graphite, SiC, Si_3N_4 and AlN.

2. Review of threshold displacement energy measurements.

The most important physical parameter for describing radiation damage in a material is the threshold displacement energy, which is simply the minimum amount of transferred kinetic energy to a lattice atom that results in the formation of a stable Frenkel pair. Since ceramics generally consist of multiple sublattices, this parameter must be separately measured for each sublattice. In addition, measurements must be obtained for different crystallographic orientations since the displacement energy is dependent on orientation. Numerous studies on the threshold displacement energies in ceramics have been performed over the past 35 years. Many of the published results up to 1985 have been summarized in previous review papers [1,5,7,8]. Additional work published since 1985, along with results obtained in older studies not previously reviewed, suggest that the displacement energies in several ceramics should be revised from the values recommended by Clinard and Hobbs [8].

Almost all of the threshold displacement energy (E_d) measurements have utilized electron irradiation sources to produce isolated point defects. Many of the studies have used optical spectroscopy or EPR techniques to uniquely monitor the behavior of a particular defect such as an anion vacancy. However, in some cases it has been reported that the EPR or optical signal may not be visible unless displacement damage occurs on both sublattices [10]. An alternative technique utilizes in situ monitoring of defect cluster formation or amorphization in a transmission electron microscope. It is generally assumed in the TEM studies that visible damage requires displacement of defects from all of the sublattices. Therefore, the measured threshold electron energy for creation of damage generally corresponds to the minimum energy to displace the most massive atomic species in the ceramic (or alternatively the sublattice with the highest E_d if the masses are comparable). This assumption has been verified to be correct in several cases, e.g., [11].

The most accurate technique for determining E_d is to experimentally bracket the threshold electron irradiation energy required to produce point defects. The relationship between E_d and the threshold electron energy is given by the following well known equation

$$E_d = \frac{2E_e(E_e + 2m_e c^2)}{mc^2} = \frac{2147.7E_e(E_e + 1.022)}{A}, \quad (1)$$

where E_d is in eV, E_e is in MeV and A is the atomic mass of the displaced ion in the right hand side of the equation. Several studies have estimated E_d by performing electron irradiations at energies above the threshold value, and comparing the measured point defect concentration with the theoretical (modified Kinchin–Pease) concentration. This latter technique typically overestimates E_d, since the irradiations are often performed at temperatures where interstitials are mobile (> 50–200 K for most ceramics, see Section 3.1) and thereby recombine with many of the vacancies. Several studies have examined the effect of irradiation temperature on E_d. According to previous studies performed on metals, e.g., [12], E_d decreases steadily with increasing temperature. However, threshold displacement energy measurements on Al_2O_3 and MgO indicate that E_d is approximately constant over the temperature range between 78 K and 400 K [5,13,14]. Several in situ TEM studies on Al_2O_3 and MgO have observed an apparent decrease in E_d at higher temperatures [13,15,16], although it appears likely that this is due to a change in the defect aggregation process as opposed to a decrease in E_d [13,16].

One potential complication in multi-atomic ceramics occurs if the displacement energy for the lower-mass sublattice is less than or comparable to the displacement energy for the higher-mass sublattice. Depending on the specific displacement energies and ion masses, it may be possible to induce displacements of the heavy ions by a two-step collision process involving electron collisions with the light ions at lower electron energies than the direct electron–heavy ion collision sequence [17,18], thereby producing anomalously low apparent E_d values for the heavier ion. The maximum amount of energy that can be transferred from the light ion (atomic mass A_1) to the heavy ion (A_2) is $4A_1A_2E_1/(A_1 + A_2)^2$, where E_1 is the kinetic energy of the light ion. For example, assuming threshold displacement energies of 25 eV for both the oxygen and beryllium sublattices in BeO, the threshold electron energy for direct displacement of oxygen ions is 160 keV whereas the threshold electron energy for the electron–beryllium–oxygen displacement sequence is 103 keV. Therefore, an incorrect oxygen threshold displacement energy of 16 eV would be obtained for BeO if the electron–beryllium-oxygen displacement sequence was ignored. In ceramics where this two-step displacement sequence is important, an accurate measurement of the threshold displacement energy for the heavy ion can only be obtained by measuring the defect production cross-section over a wide range of electron energies (at low temperatures where defect migration does not occur). The two-step displacement sequence is apparently important for near-threshold displacements of the heavier ion in UO_2, BeO and SiC, whereas it is apparently not significant in Al_2O_3 and MgO.

Table 1 summarizes threshold displacement energy data for Al_2O_3 [14,16,19–24], MgO [11,13–15,25,26],

$MgAl_2O_4$ [27], ZnO [10,28,29], CaO [14], UO_2 [30] and BeO [31–34]. The optical absorption measurements of the aluminum sublattice threshold displacement energy in Al_2O_3 all indicate a value of ~ 20 eV [16,19,23]. The upper limits for the Al sublattice E_d values from the TEM studies (obtained by assuming that electron–ion displacements occurred on both sublattices when loop formation was visible) also suggest a value below 25–30 eV [20,22]. The oxygen sublattice measurements for Al_2O_3 fall into two groups of ~ 50 eV and ~ 75 eV. The source of this difference in measured values is uncertain, since each grouping contains both TEM and optical spectroscopy measurements. Unfortunately, the crystallographic orientation was not monitored for the optical studies by Caulfield et al. which reported $E_d = 51$ eV [14]. An upper limit for the oxygen sublattice E_d of 70 eV was obtained by Compton and Arnold by comparing the calculated and observed F center concentrations in sapphire irradiated with 0.5–1.5 MeV electrons at 77 K [21]. Townsend reported that oxygen vacancies were readily produced by 300 keV electrons in sapphire oriented with the c-axis in the plane of the foil, which gives an upper bound for E_d of 52 eV [24]. As suggested by Das [22], it is possible that the relatively high oxygen threshold reported for the TEM studies by Pells et al. [16,23] may be due to the relatively low doses in their experiments. Indeed, a similar TEM study by Pells on MgO found that the apparent E_d decreased by $\sim 20\%$ when longer irradiation times were used [13]. It is also worth noting that the electron fluences for the optical absorption studies that reported $E_d \sim 75$ eV were typically $\sim 10^{22}$ e^-/m^2 [16,19,23]. A previous optical absorption E_d study on MgO found that electron fluences of $\sim 10^{23}$ e^-/m^2 were necessary to obtain measurable defect concentrations near the threshold energy [25]. Therefore, it appears likely that the oxygen threshold displacement energy for low-index crystal orientations in alumina is approximately 50 eV.

The experimental data on MgO are in general agreement that the threshold displacement energy is about 50–55 eV for both the magnesium and oxygen sublattices (Table 1). In the TEM measurements by Pells [13], a Mg displacement energy of ~ 60 eV was observed for three different

Table 1
Summary of experimental and calculated threshold displacement energies in Al_2O_3 [14,16,19–24], MgO [11,13–15,25,26], $MgAl_2O_4$ [27], ZnO [10,28,29], CaO [14], UO_2 [30] and BeO [31–34]

Material	Threshold displacement energy (eV)		Method	Reference
Al_2O_3		$E_d^O = 51$	luminescence	Caulfield et al., 1995
Al_2O_3	$E_d^{Al} < 30$	$E_d^O = 50$ [0001]	TEM (loops)	Barnard, 1977
Al_2O_3	$E_d^{Al} < 32$	$E_d^O = 53$ [0001]	TEM (loops)	Das, 1983
Al_2O_3	$E_d^{Al} < 24$	$E_d^O = 41$ [11$\bar{2}$0]	TEM (loops)	Das, 1983
Al_2O_3		$E_d^O < 52$	optical abs.	Townsend, 1961
Al_2O_3		$E_d^O < 70$	optical abs.	Compton and Arnold, 1961
Al_2O_3	$E_d^{Al} \sim 24$	$E_d^O = 79$ [0001]	optical abs.	Agnew, 1992
Al_2O_3	$E_d^{Al} \sim 18$	$E_d^O = 75$ [0001]	optical abs. TEM	Pells and Phillips, 1979
Al_2O_3	$E_d^{Al} = 18$	$E_d^O = 76$ [0001]	optical abs. TEM	Pells and Stathopoulos, 1983
MgO	$E_d^{Mg} = 52$	$E_d^O = 55$	luminescence	Caulleld et al., 1995
MgO		$E_d^O = 53$ [001]	optical abs.	
MgO	$E_d^{Mg} = 46$–60	$E_d^O \sim 44$ [001]	TEM (loops)	Pells, 1982
MgO	$E_d^{Mg} = 51$–60	$E_d^O \sim 64$ [011]	TEM (loops)	Pells, 1982
MgO	$E_d^{Mg} = 51$–60	$E_d^O \sim 46$ [111]	TEM (loops)	Pells, 1982
MgO	$E_d^{Mg} = 61$ [001]		TEM (loops)	Youngman et al., 1980
MgO	$E_d^{Mg} = 64$ [001]		TEM (loops)	Sharp and Rumsby, 1973
MgO		$E_d^O = 60$ [001]	optical abs.	Chen et al., 1970
MgO	$E_d^{Mg} = 125$	$E_d^O = 160$ [001]	MD calc.	Sonoda et al., 1995
MgO	$E_d^{Mg} = 200$	$E_d^O = 200$ [011]	MD calc.	Sonoda et al., 1995
$MgAl_2O_4$		$E_d^O = 59$	optical abs.	Summers et al., 1980
ZnO	$E_d^{Zn} = 56$	$E_d^O = 55$ [0001]	resistivity, ESR	Locker and Meese, 1972
ZnO	$E_d^{Zn} = 70$	$E_d^O = 55$ [0001]	TEM (loops)	Yoshiie et al., 1979
ZnO	$E_d^{Zn} = 40$ [11$\bar{2}$0]		TEM (loops)	Yoshiie et al., 1979
ZnO		$E_d^O > 47$	luminescence	Garcia et al., 1987
CaO		$E_d^O = 58$	luminescence	Caulfield et al., 1995
UO_2	$E_d^U = 40$	$E_d^O = 20$	HVEM	Soullard and Alamo, 1978
BeO	$E_d^{Be} < 21$	$E_d^O \sim 23$?	TEM (loops)	Bowen et al., 1962
BeO	$E_d^{Be} < 21$	$E_d^O \sim 23$?	TEM (loops)	Wilks and Clarke, 1964
BeO	$E_d^{Be} < 27$	$E_d^O \sim 29$?	TEM (loops)	Cowley, 1966
BeO		$E_d^O \sim 76$? [0001]	optical abs.	Pigg et al., 1973

orientations at the 'standard' irradiation dose of $\sim 3 \times 10^{26}$ e^-/m^2, whereas lower apparent thresholds of 46–51 eV were obtained at three to five times higher doses. However, it is possible that the defects observed at the higher doses may be associated with oxygen loss due to surface sputtering [13]. An estimate for the oxygen sublattice E_d was also obtained in the TEM study by Pells by examining the temperature dependence of the threshold electron energy to produce visible damage. It was proposed that dislocation loop formation in MgO could occur at temperatures above ~ 500 K by a process involving oxygen ion displacements combined with thermally activated diffusion of Mg ions (i.e., no direct Mg displacements). Using this model, the observed minima in the temperature-dependent threshold energy curves at ~ 700 K were taken to represent displacement of oxygen ions with a resultant oxygen sublattice E_d of ~ 45 to 65 eV for the different crystal orientations [13]. A luminescence study by Caulfield et al. reported Mg and O sublattice E_d values of 52 and 55 eV, respectively [14], but unfortunately the crystal orientation was not monitored. Table 1 also summarizes the results of the Mg and O displacement energies calculated by a molecular dynamics (MD) code for a temperature of 0 K [26]. The calculated values are considerably higher than the experimental data, suggesting that the interatomic potential used in the calculation might not be reliable at these energies. It was also proposed that the Frenkel pairs may be more likely to spontaneously recombine at low temperatures [26].

Relatively few displacement energy studies have been performed on oxide ceramics other than Al_2O_3 or MgO. Only one known study has been performed on $MgAl_2O_4$ [27]. The E_d for the oxygen sublattice in spinel was measured to be 59 eV for an irradiation temperature of 77 K, which agrees well with the results obtained on MgO and Al_2O_3 (Table 1). A significantly higher apparent oxygen threshold energy was observed for electron irradiation of spinel at room temperature, possibly due to a larger spontaneous point defect recombination volume at the higher temperature [27]. Several different sets of threshold displacement energy measurements have been reported for ZnO [10,28,29]. The data indicate that the oxygen E_d is about 55 eV. Significant differences occur in the Zn sublattice data, although it may be concluded that the Zn E_d is ~ 50 to 60 eV. Both non-stoichiometric (excess Zn) and stoichiometric ZnO specimens were examined in the TEM studies in order to selectively examine defects on the anion and cation sublattices [29]. Despite numerous radiation effects studies performed on CaO [35], there has apparently been only one experimental measurement of the threshold displacement energy. Caulfield et al. reported an oxygen sublattice E_d of 58 eV in CaO at temperatures between 80 and 300 K for an unspecified crystal orientation [14]. In the only known study on UO_2, displacement energies of 40 eV and 20 eV were obtained for the uranium and oxygen sublattices, respectively, from an analysis of the defect cluster formation behavior during high voltage electron microscope irradiation [30]. Further studies are needed in order to complete and confirm the limited E_d data for $MgAl_2O_4$, CaO and UO_2.

The apparent conflicting displacement energies measured for the oxygen sublattice in BeO provide a good example of the potential experimental difficulties in displacement energy measurements. Several TEM studies have demonstrated that dislocation loop formation on both basal and prism habit planes can be induced in BeO at room temperature by 80 to 100 keV electron irradiation, whereas loops were not observed for electron energies less than 80 keV [31–33,36]. This corresponds to a Be sublattice E_d of ~ 20 to 25 eV or an O sublattice E_d of ~ 12 to 15 eV, assuming direct displacements from the electron beam. Alternatively, if it is assumed that the oxygen ions are displaced via a two-step sequence involving the lighter Be ions, then the corresponding oxygen threshold E_d is ~ 25 eV (Table 1). An optical absorption study reported an electron threshold of ~ 400 keV in BeO for defect bands occurring at 6.5 and 5.4 eV [34]. Subsequent studies have attributed these defect bands to F and F^+ centers, respectively [37,38], which would imply that the oxygen threshold E_d is ~ 76 eV. There are several possible explanations for the large discrepancy between the apparent oxygen displacement thresholds measured in the TEM and optical absorption studies. First, the evidence supporting the assignment of the 6.5 and 5.4 eV absorption bands to oxygen vacancies is not definitive and it is possible that these bands are due to defect clusters [34]. In addition, the electron fluences used in the optical absorption study ($\sim 10^{21}$–$10^{22}/m^2$) may have been too low to accurately detect the presence of the 6.5 eV absorption band above the ionization-induced background absorption, particularly at low electron energies. Therefore, the actual threshold electron energy for creation of the 6.5 eV band might be much less than 400 keV. Alternatively, it is possible that the Be sublattice E_d is ~ 20 to 25 eV and that the oxygen ions in the TEM studies were displaced by a triple ionization (Varley) mechanism which is particularly effective at the relatively low electron energies (~ 100 keV) used in the electron microscope investigations [32]. This would have produced low apparent oxygen threshold energies in the TEM studies. A semiempirical calculation by Van Vechten predicts BeO displacement energies of 28 eV and 64 eV for the Be and O sublattice, respectively [39].

As summarized in Table 2, numerous threshold displacement energy measurements have been performed on graphite [40–47], diamond [48–52] and SiC [53–60]. Much of the experimental data for graphite has been reviewed elsewhere [45,61]. Data obtained by several different experimental techniques are in agreement that the threshold displacement energy is $E_d \sim 30$ eV in graphite for low-index crystal orientations. A recent MD simulation also reported a similar average value of $E_d \sim 34$ eV in graphite [47].

There have been four known experimental measurements of the threshold displacement energy in diamond. An early measurement by Clark et al. suggested $E_d \sim 80$ eV, based on a comparison of calculated and observed (optical absorption, resistivity) defect concentrations at electron energies between 0.3 and 1 MeV [51]. This estimate must be considered an upper limit for E_d, since they did not account for point defect recombination by interstitials which would have been mobile during the room temperature irradiation [62–64] and they also apparently did not correct for the electron energy loss in the 150 μm Al foil that was placed in front of their specimen, which would have produced an energy loss of more than 0.2 MeV. A subsequent study by Bourgoin and Massarani at electron energies of 0.25–1.0 MeV suggested that $E_d \sim 35$ eV, based on electrical resistivity measurements performed at 15 K, where interstitials are not mobile [49]. However, the possible effect of displacement of boron atoms in their B-doped specimens on the measured threshold energy was not considered. A displacement energy of 55 eV was estimated from swelling (step-height) measurements of diamond irradiated with 170 keV ions at 370 K, using a simplistic model for interstitial–vacancy recombination which ignored the possibility of interstitial clustering, etc. [52]. The authors noted that 55 eV was probably an overestimate of E_d, since lattice relaxation around vacancies had not been considered in their calculation of the residual vacancy concentration from the swelling data. The most accurate determination of E_d for diamond (and the only study on diamond which used an energy bracketing technique) was obtained in a recent room temperature TEM study by Koike et al., who found values between 38 and 48 eV for different orientations [48]. A recent MD simulation has reported E_d values of 50 to 60 eV [50], which is somewhat higher than the most accurate experimental measurements.

Several studies of the threshold displacement energies in SiC have been performed, but further work is still needed to verify the accuracy of these data. An estimate for the carbon sublattice E_d has been obtained in three different studies, which all suggest a value of about 20 eV. Barry et al. obtained a carbon E_d of 22 eV in α-SiC at room temperature by measuring the carrier lifetime in a SiC light-emitting diode irradiated with 0.125–2.0 MeV

Table 2
Summary of experimental and calculated threshold displacement energies in graphite [40–47], diamond [48–52] and SiC [53–60]

Material	Threshold displacement energy (eV)		Method	Reference
graphite	$E_d^C = 20$–30		TEM (HREM)	Lulli et al., 1995
graphite	$E_d^C = 34$ [0001]		Auger spectrosc.	Marton et al., 1993
graphite	$E_d^C = 27$ [0001]		eln. amorphiz.	Abe et al., 1995
graphite	$E_d^C = 31$ [0001]		e^- irr. etch pits	Montet and Myers, 1970
graphite	$E_d^C = 34$ [0001]		TEM (def. clust.)	Egerton, 1977
graphite	$E_d^C = 23$–31 [0001]		resistivity	Iwata and Nihara, 1971
graphite	$E_d^C = 30$–42 [11$\bar{2}$0]		resistivity	Iwata and Nihara, 1971
graphite	$E_d^C = 30$ (several orientations)		TEM	Koike and Pedraza, 1993
graphite	$E_d^C = 34$ (polar avg.)		MD calc.	Smith and Beardmore, 1996
diamond	$E_d^C = 38$ [001]		TEM (def. clust.)	Koike et al., 1992
diamond	$E_d^C = 48$ [011]		TEM (def. clust.)	Koike et al., 1992
diamond	$E_d^C = 45$ [111]		TEM (def. clust.)	Koike et al., 1992
diamond	$E_d^C = 35$, 15 K		resistivity	Bourgoin and Massarani, 1976
diamond	$E_d^C < 55$, ~ 370 K		swelling	Prins et al., 1986
diamond	$E_d^C < 80$, 300 K		resistivity	Clark et al., 1961
diamond	$E_d^C = 50$ [001]		MD calc.	Wu and Fahy, 1994
diamond	$E_d^C = 50$ [011]		MD calc.	Wu and Fahy, 1994
diamond	$E_d^C = 60$ [111]		MD calc.	Wu and Fahy, 1994
SiC	$E_d^{Si} < 85$?		luminescence	Volm et al., 1994
SiC	$E_d^{Si} = 110$, 890 K		TEM (loops)	Hudson and Sheldon, 1973
SiC	$E_d^{Si} = 45$ [001]		TEM (loops)	Hønstvet et al., 1980
SiC	$E_d^{Si} = 45$ [011]		TEM (loops)	Hønstvet et al., 1980
SiC	$E_d^{Si} = 75$ [111]		TEM (loops)	Hønstvet et al., 1980
SiC	$E_d^{Si} < 60$ [0001]		TEM (amorph.)	Angelini et al., 1987
SiC	$E_d^{Si} \sim 35$?	$E_d^C = 22$? [111]	luminescence	Geiczy et al., 1971
SiC		$E_d^C = 22$	optical lifetime	Barry et al., 1991
SiC		$E_d^C < 20$	ESR	Chauvet et al., 1992
SiC	$E_d^{Si} = 35$	$E_d^C = 40$ [001]	MD calc./Tersoff pot.	Wong et al., 1994
SiC	$E_d^{Si} = 85$	$E_d^C = 30$ [011]	MD calc./Tersoff pot.	Wong et al., 1994
SiC	$E_d^{Si} = 35$	$E_d^C = 25$–50 [111]	MD calc./Tersoff pot.	Wong et al., 1994

electrons, and attributing the extrapolated damage threshold at 0.108 MeV to carbon displacements [54]. An EPR study performed on β-SiC reported that carbon vacancies were created by 0.10 MeV electron irradiation at room temperature, indicating that $E_d < 20$ eV [55]. Unfortunately, the crystal orientation was not specified in either of these two studies. Geiczy et al. used luminescence techniques to study the defects created at room temperature in β-SiC by electrons with energies between ~0.11 and 3.5 MeV [53]. Energy thresholds were observed at ~0.11 MeV and ~0.19 MeV for spectra which were tentatively suggested to be associated with C and Si defects, respectively, which corresponds to an E_d of ~22 eV for the C sublattice and ~18 eV for the Si sublattice assuming direct displacement of these ions by electrons. Assuming the more likely possibility that the Si displacements were created via a two-step collision sequence involving the carbon ions, the threshold Si displacement energy calculated for the 0.19 MeV electron–C–Si collision sequence is 35 eV. An early high voltage electron microscope (HVEM) study performed at 890 K reported a very high apparent Si displacement threshold of ~110 eV [56]. It seems possible that the high apparent displacement energy may be due to a high point defect recombination volume at this temperature, similar to the case mentioned previously for spinel. A subsequent HVEM study reported erratic behavior for irradiation temperatures above 800 K [57]. Irradiations at temperatures below 300 K were found to give very reproducible results, and the threshold electron energy determined by a bracketing technique ranged from 240 to 370 keV for different orientations. The authors associated these threshold energies with carbon displacements, rather than with the heavier Si atom [57]. However, according to the other studies summarized in Table 2, the threshold electron energy for C displacements in SiC is only ~100 keV. If the data by Hønstvet et al. [57] are attributed to direct Si displacements by the electron beam, then the Si displacement energy would be 23 to 38 eV for the different orientations. Alternatively, if the threshold energies are associated with the electron–C–Si collision sequence, then the resultant Si threshold E_d values would range from 45 to 77 eV. In another TEM study, α-SiC was observed to change to an amorphous phase during exposure to 300 keV electrons at ~80 K [58]. If it is assumed that both the Si and C atoms must be displaced in order to produce the amorphous phase, then the upper limit for the Si sublattice E_d would be 30 eV assuming direct electron–Si displacements or 60 eV assuming the more likely electron–C–Si displacement sequence. A defect tentatively proposed from photoluminescence and Zeeman spectroscopy studies to be a Si monovacancy was observed in α-SiC following 0.4 MeV electron irradiation at room temperature [59], which would imply that the Si sublattice E_d is < 43 eV assuming direct electron–Si collisions or < 85 eV assuming the electron–C–Si displacement sequence. MD calculations of the threshold displacement energies in SiC have been obtained for several different interatomic potentials [60,65,66]. The Tersoff potential gives the best fit to SiC physical parameters such as bulk modulus, melting point, etc., and is therefore considered to be more reliable than the Pearson potential [65]. Displacement energies calculated by the Tersoff potential range from 25 to 40 eV for the C sublattice and 35–85 eV for the Si sublattice [60].

Table 3 summarizes the recommended values of the threshold E_d (averaged over the low-index crystal orientations, where available) for the ceramics evaluated in this review. Based on similar work in metals, high-index crystallographic directions should have much higher displacement energies than low-index directions. Therefore, the value of the threshold displacement energies averaged over all crystal orientations should be larger than the values given in Table 3. However, there is not enough available information on the crystal orientation dependence of the displacement energy in ceramics to accurately determine the appropriate scaling parameter between the measured threshold displacement energies for low-index directions and the polar-averaged displacement energies. Considering that crystal orientation effects are probably smaller in ceramics compared to metals [67], it may be speculated that the polar-averaged E_d values (relevant for bulk radiation damage environments such as neutron irradiation)

Table 3
Recommended threshold displacement energies in ceramics

Material	Threshold displacement energy (eV)		Comments
Al_2O_3	$E_d^{Al} \sim 20$	$E_d^O = 50$	previous 'standard' value for E_d^O was 76 eV
MgO	$E_d^{Mg} = 55$	$E_d^O = 55$	good agreement among five studies
$MgAl_2O_4$		$E_d^O = 60$	only one known measurement
ZnO	$E_d^{Zn} \sim 50$	$E_d^O = 55$	moderate uncertainty in E_d^{Zn}
BeO	$E_d^{Be} \sim 25$	$E_d^O \sim 70$?	large uncertainty in data
UO_2	$E_d^U = 40$	$E_d^O = 20$	only one known measurement
SiC	$E_d^{Si} \sim 40$?	$E_d^C = 20$	large uncertainty in E_d^{Si}
Graphite	$E_d^C = 30$		extensive data base
Diamond	$E_d^C = 40$		four known measurements

would be ~ 30% larger than the values listed in Table 3. We were unable to find any published experimental or computed E_d results for the nitrogen-bearing ceramics such as AlN, Si_3N_4, or $9Al_2O_3 \cdot 5AlN$ (AlON). In addition, we did not locate any corresponding studies on ZrO_2 or Y_2O_3. A semiempirical analysis by Van Vechten predicts E_d values of 27 eV and 35 eV, respectively for the Al and N sublattices in AlN [68]. There have been some attempts to measure E_d for TiC and TiO_2, but the reported values (e.g., ~ 5 eV in Ref. [69]) are much lower than that measured in other ceramics, suggesting that the measured value is not due to elastic collisions.

Several of the recommended values in Table 3 are significantly different from the values proposed by Clinard and Hobbs [8]. In particular, the oxygen sublattice E_d value for Al_2O_3 has been reduced to ~ 50 eV from the previous recommended value of 76 eV. The new value is in better agreement with oxygen sublattice E_d values of 50–60 eV obtained on other close packed anion ceramics such as MgO, CaO, spinel and ZnO (Table 1). Our recommended E_d for diamond is one-half of the value published in the review by Clinard and Hobbs. Finally, several recent E_d measurements on SiC, along with a reevaluation of older published data, allow us to recommend E_d values that are significantly less than previously proposed values for SiC. The accuracy of the recommended E_d values are generally thought to be +5 to 10 eV, with the highest accuracy occurring in graphite and the lowest accuracy occurring in SiC and spinel. Further threshold energy measurements would clearly be valuable, in order to confirm the results recommended in Table 3 and to obtain some estimate of E_d on other technologically important ceramics such as AlN and Si_3N_4.

3. Defect production and migration

In monatomic solids, the displacement damage dose can be directly calculated from the damage energy using the well-known modified Kinchin–Pease model [70]. This model cannot be directly applied to multi-component ceramics, due to the different atomic mass and E_d values for the anion and cation sublattices. Several authors have outlined methods to calculate displacement damage in polyatomic materials that consist of multiple sublattices [71–79]. The currently-accepted standard model for calculating radiation damage in multi-component ceramic materials was developed by Parkin and Coulter about 15 years ago [76–78]. They developed a system of equations to describe the atomic displacements on different sublattices, and showed that their results could be written in a form that is analogous to the Kinchin–Pease expression for displacement damage. Unfortunately, this system of equations is complex to apply, and representative results for different irradiation spectra have only been published for a few specific cases [79–82]. Several studies have evaluated the production of displacement damage in multi-component ceramics with binary collision approximation computer codes [83,84]. Ghoniem and Chou obtained a particularly simple empirical value for an effective displacement energy in $MgAl_2O_4$ that could be used with the Norgett–Robinson–Torrens (NRT) model [70] to provide a satisfactory estimate of the total number of displacements at high PKA energies. Assuming that a similar relation holds for other ceramics, the effective displacement energy is

$$E_d^{\text{eff}} = \left[\sum_i \frac{S_i}{E_d^i} \right]^{-1}, \tag{2}$$

where S_i and E_d^i are the stoichiometric fraction and displacement energy of the ith atomic species, respectively. Using the recommended displacement energies in Table 3, the effective displacement energies for SiC, Al_2O_3, and MgO (rounded to the nearest 5 eV) are 25 eV, 30 eV and 55 eV, respectively. Considering the Coulombic nature of the collision cascade, a somewhat more appropriate scaling parameter for the effective displacement energy might be $S_i Z_i^2 / A_i$, where Z_i is the atomic number and A_i is the atomic mass of the ith atomic species.

3.1. Defect migration kinetics

Before the published studies on defect production efficiency are reviewed, it is pertinent to summarize the available information on defect migration energies in ceramics. This information is useful because it will be seen that many of the published defect production studies failed to account for point defect migration and annihilation in the evaluation of their experimental data, and therefore their published defect production efficiencies are likely an underestimate of the actual value. Since most of the defect production studies have been performed on alumina and MgO, we will concentrate on the corresponding defect migration studies for these two ceramics. Some of the published migration enthalpies for numerous ceramic materials have been summarized by Clinard and Hobbs [8].

Table 4 summarizes the published migration energies for vacancy and interstitial diffusion in MgO [26,85–94].

Table 4
Summary of experimental and calculated point defect migration energies in MgO and Al_2O_3

Material	Point defect	Migration energy (eV)	Ref.
MgO	Mg vacancy	2.0–2.3	[26,85–88]
MgO	O vacancy	2.0–2.5	[26,85,86,88,89]
MgO	Mg, O interstitials	0.5–1.5	[88,90–94]
MgO	Mg, O interstitials	≤ 0.2	[26,85,93]
Al_2O_3	Al vacancy	1.8–2.1 (< 1)	[86,104,107,108]
Al_2O_3	O vacancy	1.8–2 (1.1)	[16,86,102–104]
Al_2O_3	Al, O interstitials	0.2–0.8	[93,115,116]

There is rather good agreement in the literature regarding the migration energy for vacancy diffusion on the Mg and O sublattices. The Mg vacancy migration energy appears to be 2.0–2.3 eV, and the reported oxygen vacancy migration energy is 1.9–2.5 eV. Henderson and coworkers originally reported a Mg vacancy migration energy of 0.96 eV based on annealing studies of divacancy formation in neutron irradiated MgO [87]. However, their measured activation energy should correspond to 1/2 of the Mg vacancy migration energy, since divacancy formation from migrating vacancies is a second order process [95].

There is considerable disagreement in the literature regarding the magnitude of the interstitial migration energies in MgO, with estimates ranging from ~ 0.1 eV to ~ 1.5 eV. Several measurements of F center (oxygen vacancy) annealing in irradiated MgO specimens suggest that the oxygen interstitial migration energy is ~ 1.5 eV [90,91]. However, the irradiation temperature in one of these studies was > 320 K [90], which may have been too high to prevent interstitial migration during the irradiation. A recent calculation for oxygen interstitials in MgO reported that the migration energy decreased from ~ 1.45 eV for to O_i^- 0.5–1.2 eV for double-ionized O_i^{2-} ions [92], suggesting that high ionization levels such as that found during electron irradiation might enhance point defect migration (also see Section 4). Kingery observed significant annealing of the volumetric expansion of MgO during warming up to room temperature after neutron irradiation at 77 K [93]. He suggested that either spontaneous close-pair recombination or else Frenkel pair recombination due to interstitial migration with a range of activation energies (~ 0.2–0.8 eV) had occurred. On the other hand, Sibley and Chen did not observe any F center annealing in MgO during warmup to room temperature after neutron irradiation at 80 K [96]. Recent diffusion marker broadening measurements following Kr ion irradiation at temperatures up to ~ 900°C reported an activation energy of 0.3 to 0.35 eV for both the anion and cation sublattices [94]. The authors suggested that the kinetics were controlled by interstitial loop formation, which would imply anion and cation migration enthalpies of 0.6 to 0.7 eV for the rate-controlling (slower) species on each sublattice if the loop nucleation is a second order process. A high temperature electron irradiation experiment [85] and a recent MD calculation [26] have both reported oxygen and magnesium interstitial migration energies < 0.1 eV in MgO. Several irradiation studies on MgO by Rius et al. have provided evidence that oxygen interstitials may be mobile at temperatures < 27 K [97,98]. This conclusion regarding low-temperature mobility of oxygen interstitials in MgO is supported by separate electron [91] and proton [99] irradiation experiments performed at 4 K and 15 K, respectively, which found sublinear F center accumulation rates. Since the maximum defect concentrations were $<$ 100 appm, the sublinear behavior should not be due to saturation in the defect concentration. A more likely explanation is that uncorrelated recombination of point defects occurred during the irradiation, due to long-range migration of oxygen interstitials or impurities. Due to the highly ionizing nature of the electron and proton irradiations, it is possible that the interstitial diffusion may have been enhanced by ionization processes (cf. Section 4). Another proton irradiation study on MgO at irradiation temperatures between 88 and 300 K found that the defect production decreased rapidly with increasing temperature, with an activation energy of ~ 0.1 eV [100]. Both the electron and proton irradiation studies reported that F center annealing did not occur when the MgO specimen was warmed up to room temperature following irradiation [91,99,100]. Therefore, either oxygen interstitial migration has already occurred at the irradiation temperature (possibly assisted by ionization processes), or else interstitials are immobile below room temperature. The swelling measurements by Kingery [93] and the observed sublinear F center accumulation at low temperatures in several electron and proton irradiation studies [91,99] suggest that the first mechanism is more likely, but further work is clearly needed to resolve the issue of interstitial mobility in MgO. A further complication is that the long range migration of point defects in MgO can be strongly affected by impurities such as OH^- ions [101].

The published migration energies for vacancy and interstitial diffusion in Al_2O_3 are also summarized in Table 4. The oxygen vacancy migration energy has been reported to be ~ 1.8 eV in experimental [102,103] and theoretical [86,104] studies. Pells and Stathopoulos reported an activation energy of ~ 0.55 eV for the formation of F_2 centers from isolated F centers [16]. This corresponds to an oxygen vacancy migration energy of ~ 1.1 eV, since the nucleation process is a bimolecular (second order) reaction. It is uncertain why their measured migration energy is low compared to other measured values. Atobe and coworkers noted that F_2 center formation occurred during postirradiation annealing of neutron irradiated sapphire specimens at temperatures above ~ 180°C, but they did not measure an associated activation energy [105]. However, their results suggest that the oxygen vacancy migration energy is ~ 1 to 1.5 eV, assuming typical pre-exponential factors for the diffusion coefficient. Most studies have concluded that cation diffusion occurs with a lower activation energy than oxygen diffusion in Al_2O_3 [103,106], although there are very few experimental measurements of the Al migration energy. Theoretical calculations suggest that the Al vacancy migration energy in Al_2O_3 is 1.8 to 2.1 eV [86,104], which is comparable to the oxygen migration energy. A positron lifetime study of electron-irradiated Al_2O_3 reported that aluminum vacancy annealing occurred above 930 K, which corresponds to an activation energy of ~ 1.8–2.0 eV [107]. An early experimental measurement by Palladino and Kingery suggested an Al self diffusion energy of 4.9 eV [108], which gives an Al vacancy migration energy of < 1 eV if the calculated

Schottky formation energy of 4 to 5 eV [86,104] is subtracted. It has been suggested that this measurement was too low due to grain boundary diffusion or other extrinsic diffusion effects [86,104].

There is relatively little information available on the interstitial migration energies for Al_2O_3. Many studies have implicitly assumed that interstitials are immobile in Al_2O_3 at temperatures below 100–300°C. Annealing of F centers following irradiation near room temperature has been observed to occur at temperatures above ~ 100°C [5,105,109–111], and has generally been attributed to Frenkel pair recombination associated with long range migration of oxygen interstitials. However, several optical absorption studies have reported that the decrease in F center concentration above 200°C coincides with the formation of oxygen divacancy clusters [5,105], indicating that the F center annealing in this temperature range is due to oxygen vacancy migration rather than interstitial migration. Mixed results have been obtained regarding the minimum temperature for interstitial migration in Al_2O_3. A relatively high dose study reported that F center annealing did not occur during warmup to room temperature following ion irradiation at 77 K, suggesting that oxygen interstitials are immobile below room temperature [112]. On the other hand, annealing of F centers at room temperature has been reported in several studies for Al_2O_3 specimens irradiated at or below 300 K [21,109,111,113]. This low-temperature F center annealing has been attributed to 'close-pair' recovery [5], but a more likely explanation is that three-dimensional interstitial migration occurs at temperatures as low as ~ 200 K in Al_2O_3. Kingery reported that the lattice parameter increase in sapphire irradiated with neutrons at 77 K exhibited significant annealing at test temperatures as low as 200 K [93]. A detailed examination of the kinetics of the lattice parameter and density changes during annealing at temperatures between 200 and 400 K led to the conclusion that interstitials with a range of migration energies between 0.2 and 0.8 eV were responsible for the annealing [93]. An EPR study concluded that at least three different orientations of Al interstitials were present in Al_2O_3 following neutron irradiation at 77 K, each having different migration energies [114]. Two of the configurations were found to be unstable (mobile) below room temperature, whereas the third configuration was thermally stable at room temperature, which suggests that the Al interstitial migration energies range from ~ 0.3 to ~ 0.8 eV for the different defect states. A luminescence study on neutron irradiated Al_2O_3 reported a migration energy of 0.8 eV for Al interstitials [115]. Due to the relatively high irradiation temperatures (> 320 K), the possible presence of Al interstitial defect states with migration energies less than 0.8 eV would not have been detected in the annealing study [115] since these defects would easily migrate to sinks or form clusters during the irradiation. A recent TEM study estimated the activation energy for the rate-determining (slower) interstitial species in Al_2O_3 to be ~ 0.8 eV from an analysis of dislocation loop denuded zones adjacent to grain boundaries in ion-irradiated specimens [116]. As reviewed in Section 3.2, numerous studies have observed that the Al_2O_3 defect production rate at room temperature is approximately an order of magnitude lower than that observed at 15–77 K [24,111,112,117]. The observation of sublinear defect accumulation rates during irradiation near room temperature, e.g., Ref. [111], is a strong indication of uncorrelated recombination due to long-range migration of interstitials (cf. Section 3.2). In summary, it appears that both Al and O interstitials are mobile in Al_2O_3 below room temperature, but further work is needed to determine their migration energies. It is likely that a range of activation energies may be observed, corresponding to different orientations of the interstitial along with possible impurity trap effects.

Point defect mobilities are not well known for the other ceramics considered in this review. A brief summary of the data for diamond and SiC illustrates the magnitude of the uncertainties in the data base. Several studies have investigated the mobility of point defects in diamond [52,62–64,118]. It is generally agreed that vacancy migration occurs at temperatures above ~ 850°C [62,118]. The reported threshold temperature for thermally activated interstitial migration in diamond ranges from ~ 50–100 K [63,118] to 260–350 K [52,62,63]. The large range in reported interstitial migration temperatures is mainly associated with uncertainties about the influence of migrating impurities on experimental measurements [63]. A recent 300 keV electron irradiation study observed defect cluster formation at a temperature of 16 K [64], which implies that interstitials are mobile at this very low temperature. It appears likely that ionization-induced diffusion (cf. Section 4) may be influencing at least some of these measurements.

Most of the experimental data on SiC indicate that vacancy migration occurs with a range of activation energies at annealing temperatures between ~ 500 and 1000°C [53,119–121]. An activation energy of 2.2 eV has been reported for carbon vacancy migration [53]. Similar results have also been obtained in a recent MD simulation study, with reported activation energies of ~ 2.6 eV and 2.9 eV for carbon and silicon vacancies, respectively [65]. Vacancy annealing has been observed in irradiated SiC at temperatures near 100°C [120,121] which may be attributable to interstitials migrating to the Si vacancies. On the other hand, an older EPR study concluded that Si vacancies were mobile in pure SiC at room temperature [122]. Boron impurity trapping effects were reported to increase the effective Si vacancy migration energy to ~ 1.5 eV [122]. Very little information is known about interstitial migration in SiC. MD calculations suggest that the migration energies are ~ 1.3 eV and ~ 4 eV for carbon and silicon interstitials, respectively [65]. A recent analysis of temperature-dependent amorphization data for ion and neutron-irradiated SiC suggests that the interstitial

migration energy is ~0.6 eV [123]. It was assumed in their analysis [123] that this activation energy corresponded to the slower migrating interstitial (presumably Si).

3.2. Surviving defect (production efficiency) measurements

It is well established from experimental and theoretical studies on metals that the fraction of defects that survive in-cascade (correlated) recombination events decreases from ~100% to ~30% of the number of displacements calculated by NRT model as the average primary knock-on atom (PKA) energy increases from ~100 eV to >10 keV [124,125]. Measurement of this surviving defect fraction (also known as defect production efficiency) can only be performed at temperatures where point defects are immobile and at doses well below the level that produces a saturation in the defect concentration (typically ~0.1 at.%); otherwise, uncorrelated recombination and/or cascade overlap events interfere with the measurement and produce an underestimate of the surviving defect fraction. As established by radiation effects studies on metals, a sublinear defect accumulation rate is a clear indication that either uncorrelated recombination or cascade overlap is occurring [126].

There have been numerous attempts to measure the surviving defect fraction in MgO and Al_2O_3 irradiated with different types of particles. Almost all of these studies used optical absorption techniques to monitor the concentration of oxygen vacancies. Unfortunately, most of these irradiation studies were performed near room temperature, where it is likely that interstitials are sufficiently mobile to diffuse long distances and cause uncorrelated recombination with the oxygen vacancies (cf. Section 3.1). Fig. 1 shows an example of the dose-dependent oxygen vacancy accumulation behavior for Al_2O_3 irradiated with neutrons at 15 K and 360 K [111]. A constant factor of 1 dpa = 1×10^{25} n/m^2 ($E > 0.1$ MeV) was used to convert the original fluence values to a displacement damage level in this figure. The optical absorption measurements were made at room temperature, so it is possible that some F-center annealing may have occurred in the specimen irradiated at 15 K prior to the data acquisition. However, the main feature of importance is that the defect accumulation rate was sublinear with dose for the specimen irradiated at 360 K whereas a linear accumulation rate was obtained for the specimen irradiated at 15 K. It is difficult to imagine that cascade overlap effects could be responsible for the sublinear behavior in the 360 K specimen, since the maximum defect concentration was <10 appm and the maximum dose was <0.0004 dpa. The observed square root dose dependence for the F center accumulation at 360 K is in accordance with the predictions of the 'unsaturable trap model' for defect accumulation that has been used to explain uncorrelated recombination processes in irradiated metals [126]. Application of this model to the 360 K data gives an estimate for the mobile oxygen interstitial fraction (relative to the NRT value) of $f \sim 20\%$. However, it is unlikely that such a simplistic model (or other models developed primarily for metals, e.g., [127–129]) could accurately model the physical processes occurring in an irradiated ceramic consisting of multiple sublattices. From the linear defect accumulation rate obtained on the specimen irradiated at 15 K, it can be inferred that the oxygen monovacancy concentration is ~10% of the calculated NRT value. This is a lower limit to the surviving defect fraction, since some defects may have been annihilated during the warmup to room temperature and defect clusters (divacancies, etc.) are not included in this measurement. Several optical absorption studies have concluded that the defect cluster concentration is typically much less than the monovacancy (F center) concentration for neutron irradiated MgO or Al_2O_3 at temperatures below 400 K [5,105,130]. On the other hand, significant concentrations of a defect with a 574 nm absorption band tentatively identified as an oxygen divacancy [130,131] have been observed in MgO irradiated with fission neutrons near 350 K [132]. The concentration of this divacancy center was significantly greater than that for the F center over a wide dose range of ~0.0001–0.1 dpa.

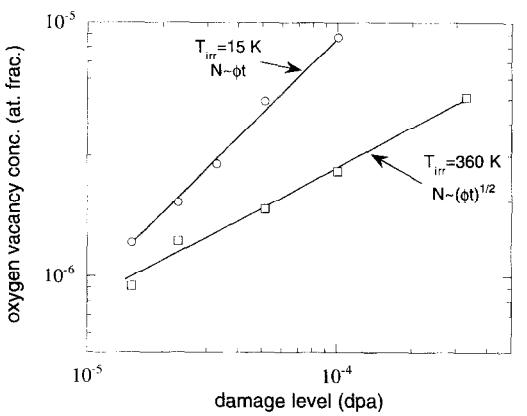

Fig. 1. Dose-dependent F center concentration measured at room temperature in sapphire after fission reactor irradiation at 15 K and 360 K [111].

Fig. 2 shows the dose-dependent F center concentration in MgO irradiated with either fission or D–T fusion (14 MeV) neutrons near room temperature [133]. Conversion factors of 1 dpa = 1×10^{25} n/m^2 ($E > 0.1$ MeV) and 1 dpa = 0.5×10^{25} n/m^2 ($E = 14$ MeV) were used to convert the original fluence values to displacement damage doses in this figure. It can be seen that both the fission and fusion data exhibited approximately linear behavior up to ~10^{-4} dpa (~10 appm vacancy concentration), and a square root dose dependence was observed at higher doses. From the slope of the low-dose region, the oxygen monovacancy concentration is seen to be ~10% of the calculated NRT value. Application of the unsaturable trap model

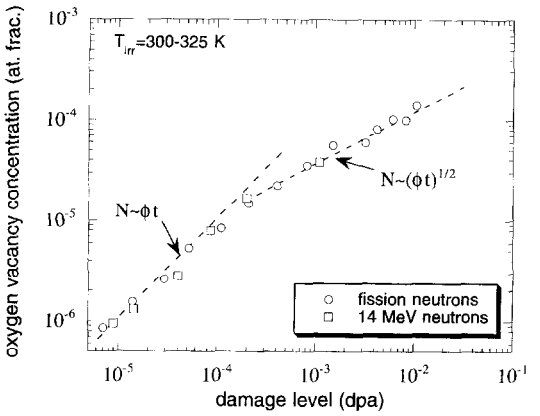

Fig. 2. Dose-dependent F center concentration measured in MgO after fission reactor or 14 MeV neutron irradiation near room temperature [133].

[126] over the linear and square root regions of the plot yields an estimate for the mobile oxygen interstitial fraction of ~8% for the fission data and ~9% for the 14 MeV neutron data. Although these latter values are in good agreement with the low dose (linear accumulation) results, it must be reiterated that the validity of a simplistic model such as the unsaturable trap model for ceramic materials is uncertain. All of these measurements must be considered as lower limits to the surviving defect fraction since correlated point defect recombination has probably occurred, and defects contained in clusters were not counted.

Numerous studies have reported that the point defect accumulation rates obtained from F center measurements on MgO [91,99,100,134] and Al_2O_3 [5,24,111,112,117, 134,135] are about an order of magnitude higher for irradiation at cryogenic temperatures (4–77 K) compared to room temperature. Unfortunately, many authors did not investigate the possibility of sublinear defect accumulation rates, so the quantitative accuracy of the reported room temperature values is uncertain. In some cases, the authors noted sublinear behavior but still quoted an average survival fraction (obtained from the quotient of the observed defect concentration and the dpa level).

The published surviving defect fraction measurements on Al_2O_3 irradiated at cryogenic temperatures are summarized in Fig. 3 [93,111,112,134,135]. Data obtained at irradiation temperatures > 290 K were not included in this plot, since it is likely that interstitials are mobile at these temperatures and would reduce the apparent surviving defect fraction via correlated and uncorrelated recombination. Most of the data in Fig. 3 were obtained from F center measurements, and therefore do not include surviving defects that have clustered (divacancies, etc.). The cryogenic density measurements by Kingery [93] were converted into a surviving defect fraction by assuming a Frenkel pair relaxation volume of 1 atomic volume and assuming a neutron fluence conversion of 1×10^{25} n/m^2 ($E > 1$ MeV) ~ 2 dpa. The F center measurements by Averback et al. [134] were performed at room temperature following ion irradiation at 77 K, so some defect annealing may have occurred. Considerable variability exists in the data, but the apparent surviving defect fraction in Al_2O_3 is ~30% of the modified Kinchin–Pease calculated displacements at all PKA energies between 0.1 and 90 keV. This result is in contrast to defect production measurements on light metals such as aluminum (also plotted in Fig. 3) which observed a steady decrease in the surviving defect fraction from ~100% to ~50% as the average PKA energy increased from ~0.5 keV to ~50 keV [124]. The relatively low surviving defect fraction measured in Al_2O_3 compared to Al may be attributable to either a larger spontaneous recombination volume or more likely, the presence of a significant amount of clustered defects which were not detected in the F center measurements. It is also possible that at least some interstitial configurations in Al_2O_3 may be mobile at 80 K, which would inevitably lead to some point defect recombination and thereby reduce the measured surviving defect fraction. The experimental measurements on Al were performed at temperatures below 10 K.

Estimates of the surviving defect fraction in MgO obtained from measurements on specimens irradiated at 4–80 K are summarized in Fig. 4 [91,93,99,112,134,136]. Once again, the data by Averback et al. [134] may be an underestimate of the surviving defect fraction since their optical measurements were performed at room temperature. The MgO density change data by Kingery [93] were converted into a surviving defect fraction using the same assumptions as for his alumina data. The measured surviving defect fraction in MgO does not exhibit any noticeable dependence of PKA energy between 0.1 and 90 keV. This behavior is similar to the results for Al_2O_3 (Fig. 3), but is

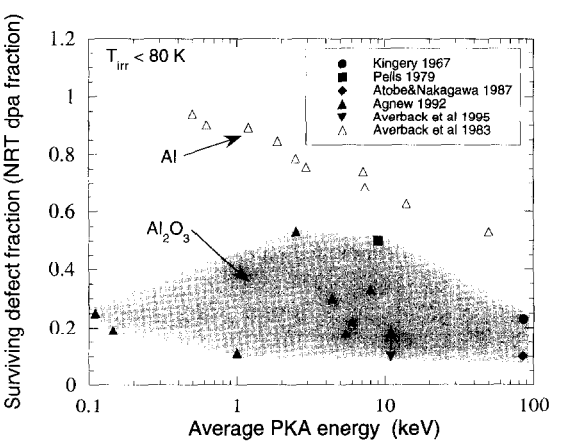

Fig. 3. Surviving defect fraction in Al_2O_3 irradiated at cryogenic temperatures, as obtained from F center [111,112,134,135] and density change [93] measurements. Data obtained on irradiated Al [124] are shown for comparison.

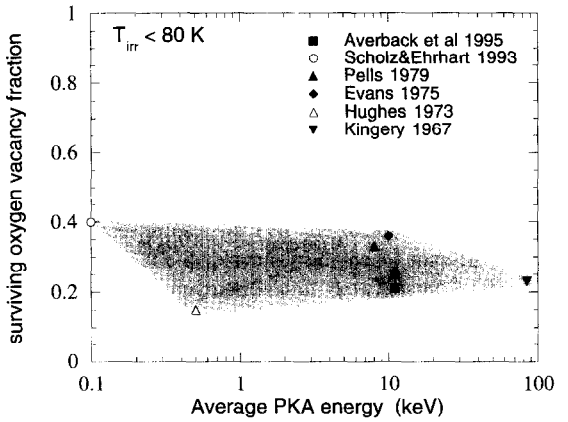

Fig. 4. Surviving defect fraction in MgO irradiated at cryogenic temperatures, as obtained from F center [91,99,112,134,136] and density change [93] measurements. The F center measurements by Averback et al. [134] were performed at room temperature and therefore represent a lower limit to the surviving defect fraction due to possible annealing.

in sharp disagreement with the results obtained at low temperatures on aluminum and other metals [125]. MD calculations performed on MgO indicate that the spontaneous point defect recombination volume is only slightly larger (by ~ 50%) than typical values for metals [26]. Therefore, the defect production efficiency versus PKA energy for MgO would be expected to be qualitatively similar to that observed in metals. Further measurements on MgO and Al_2O_3 at temperatures near 4 K are needed to determine if the apparent independence of the surviving defect fraction on PKA energy is an experimental artifact. As discussed in the following section, the possible influence of ionization-induced diffusion and ionization-enhanced point defect recombination also needs to be considered in the analysis of the defect production efficiency data, particularly at low PKA energies where the concentration of ionized defects per displacement is relatively high.

4. Role of subthreshold irradiation on microstructural evolution

Several significant radiation effects can occur in ceramics from exposure to irradiation particles that are not sufficiently energetic to produce displacement damage by elastic collisions, i.e., subthreshold energy irradiations. It is well known that ionizing radiation can efficiently produce displacement damage in numerous inorganic insulators, including alkali halides, silica, and various hydrides, carbonates, chlorates, bromates and silicates [1,3,8]. On the other hand, displacement damage by ionizing radiation has not been observed in crystalline oxide or nitride ceramics such as MgO, Al_2O_3, AlN or Si_3N_4 [8,137]. Several studies have noted that intense beams of ionizing radiation such as that found in field-emission-gun electron microscopes can cause reduction of oxides [138–141]. This reduction and accompanying desorption can lead to surface faceting and 'hole-drilling' in the electron-irradiated region. It has been demonstrated that this phenomenon is due to ionization processes rather than atomic collisions [139,140], and the process is accelerated at elevated temperatures [141,142]. Models such as the Knotek–Feibelman radiolytic mechanism [143,144] have been proposed to explain these effects, and it has been suggested that several ionization mechanisms may be simultaneously operating [139,140]. It has also been proposed that multiple ionization self trapped exciton processes may promote the surface desorption of oxygen in intensely ionizing radiation environments [145]. For the purposes of this review, it is worth noting that ionization-induced reduction of ceramics such as Al_2O_3 and MgO is generally only of importance in high-dose studies of thin films that utilize highly ionizing radiation sources.

Another important process in semiconductors and insulators associated with irradiation sources that deposit significant amounts of energy via ionization or subthreshold elastic collisions is the enhancement of point defect diffusion [2,146,147]. This enhancement in diffusion occurs in bulk specimens as well as thin films, and therefore can have a potential impact on all radiation effects studies on ceramics. It has generally been assumed that the enhancement in diffusion is due to ionization effects, although in some cases it is possible that subthreshold elastic collisions may also be assisting the point defect diffusion. Early work by Walker demonstrated that neutron-induced point defect swelling in BeO could be substantially annealed by exposure to 1 MeV electrons at 100°C [148]. Subsequent studies on Al_2O_3 and MgO reported that proton or 8 keV electron irradiation could anneal the volume expansion created by prior heavy ion irradiation [149–151]. Further confirmation of point defect annealing in MgO and Al_2O_3 by subsequent subthreshold irradiation has been recently obtained by several other research groups [91,134,152]. These results suggest that ionizing radiation can stimulate annealing of close Frenkel pairs. The subthreshold irradiation-stimulated annealing process in these oxides was observed to be enhanced at higher irradiation temperatures [134].

Several additional experimental observations have demonstrated that subthreshold irradiation can promote point defect diffusion in ceramics. An ordered array of cavities was observed in alumina irradiated with simultaneous triple ion beams (H, He, Al) at room temperature [153], indicating that significant vacancy diffusion occurred at temperatures well below the reported temperature for vacancy migration in alumina (Section 3.1). The diffusivity of hydrogen isotopes was observed to be significantly increased by ionizing radiation in a wide range of oxide ceramics [154,155]. Recent work on Al_2O_3 and BeO

has reaffirmed the presence of ion beam induced desorption of deuterium [156]. The enhancement in deuterium desorption during 1 to 2 MeV He ion irradiation was tentatively attributed to an increase in the bulk diffusivity, although radiation-enhanced surface detrapping was also considered to be a possible explanation. Several different research groups have demonstrated that room temperature ion beam amorphization can be inhibited in several ceramic insulators [157,158] and semiconductors [159] by simultaneous irradiation with electrons or light ions, and it has also been shown that subthreshold electron irradiation can enhance the recrystallization of amorphous oxide ceramics [160] and semiconductors [159,161]. Both electronic excitation (ionization) and subthreshold energy transfer mechanisms have been proposed to explain the observed inhibition of amorphization by low-energy electron beams [159,161]. In contrast, it is worth noting that ionizing radiation apparently has an insignificant effect on the amorphization behavior of SiC [157].

Recent work on ion-irradiated $MgAl_2O_4$, Al_2O_3 and MgO has found that dislocation loop nucleation is suppressed and loop growth is enhanced for light ion irradiations compared to heavy ion irradiations [116,162–164]. Figs. 5 and 6 show the loop density and size measured in Al_2O_3 specimens irradiated at 650°C with ions ranging from 1 MeV H to 3.6 MeV Fe [164]. The loop measurements are plotted as a function of the electronic to nuclear stopping power (ENSP) ratio, which is a rough measure of the amount of ionization per displaced atom [162]. It can be seen that the Al_2O_3 loop size and density are roughly independent of changes in the irradiation spectrum until the ENSP ratio approaches a value of about 1000, which corresponds to the production of $\sim 10^4$ electron–hole pairs per dpa. At ENSP ratios above ~ 1000, the loop density decreased and the size increased. Qualitatively similar behavior was also observed for MgO and $MgAl_2O_4$, although the transition occurred at ENSP ratios of ~ 400 and ~ 10, which corresponds to ~ 1000 and ~ 100 electron–hole pairs/dpa, respectively [116,163]. The observation of dislocation loop coarsening above a critical ENSP ratio is evidence for enhanced interstitial diffusion from ionization processes. An additional possible effect associated with the light ion irradiations is an ionization-enhanced increase in the spontaneous recombination volume of Frenkel defects within the displacement cascade [165]. However, the increase in dislocation loop size for the light ion irradiations indicates that a significant concentration of point defects escape recombination. Therefore, the dominant irradiation spectrum effect appears to be an enhancement in the point defect diffusion for highly ionizing radiation environments.

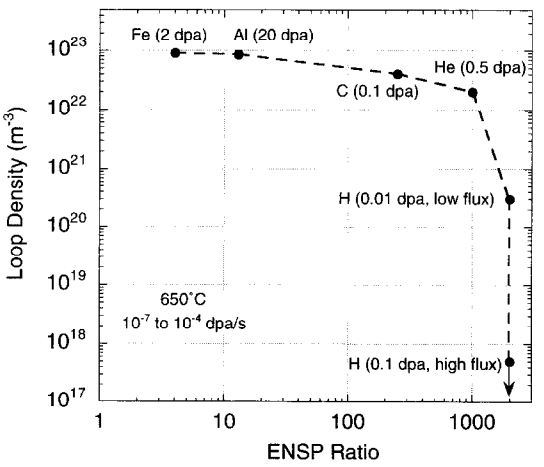

Fig. 5. Effect of irradiation spectrum (electronic to nuclear stopping power ratio) on the loop density in Al_2O_3 irradiated with single ion beams at 650°C [164].

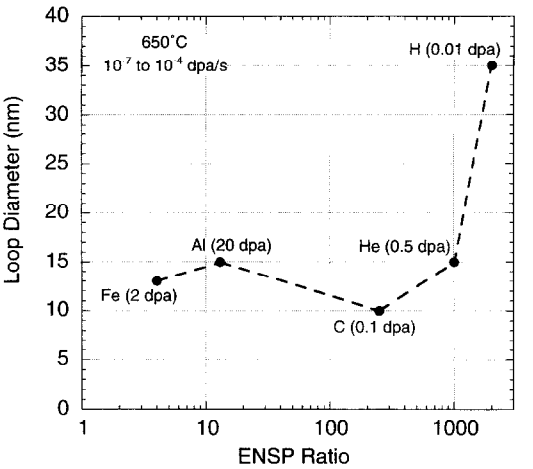

Fig. 6. Effect of irradiation spectrum (electronic to nuclear stopping power ratio) on the loop size in Al_2O_3 irradiated with single ion beams at 650°C [164].

One disadvantage associated with the single beam ion irradiation experiments is that the average PKA energy decreases for the light ion irradiations. Therefore, it is possible that the observed decrease in loop density for the light ion irradiations may be partially due to production of an increasing proportion of isolated point defects (as opposed to defect clusters). Whereas the surviving defect fraction measurements summarized in Figs. 3 and 4 indicate that the defect production efficiency does not vary strongly with PKA energy, it must be recognized that homogeneous nucleation of dislocation loops by isolated point defects would be more difficult compared to heterogeneous nucleation on defect clusters formed directly in the displacement cascade. Homogeneous loop nucleation would be even more difficult if ionization-enhanced point defect recombination occurs. A limited number of simultaneous dual beam irradiations have been performed on

spinel, in an attempt to separate PKA spectrum and ionizing radiation effects [116,163,166]. The dual beam results at 650°C indicate that the density of dislocation loops produced by medium-mass ions is unaffected by uniform ionizing radiation until the global ENSP ratio exceeds ~ 100, i.e., a factor 10 higher than found for the single ion beam irradiations [163]. This observation suggests that PKA spectrum effects (or else the location of the ionization relative to the displacement damage) may have some influence on the microstructural development. However, ionizing radiation exerts a dominant effect at high ionizing dose rates (ENSP ratio > 100 in this case). Yasuda et al. have also obtained some evidence that the suppression in dislocation loop nucleation in spinel scales better with total ionizing radiation flux rather than the ENSP ratio [166].

It is worthwhile to point out the fundamental difference between radiation-induced diffusion in ceramics, associated with subthreshold irradiation, and the well-known process of radiation-enhanced diffusion. Ignoring contributions from clusters such as divacancies, the diffusion coefficient can be written as $D = f_v D_v C_v + f_i D_i C_i$, where $f_{i,v}$ are geometric correlation factors which have values near unity and $C_{i,v}$ are the atomic concentrations of interstitials and vacancies, respectively [127]. The interstitial and vacancy diffusion coefficients are given by

$$D_{i,v} = a_o^2 \nu_{i,v} \exp - \frac{E^m_{i,v}}{kT}, \tag{3}$$

where a_o is the lattice jump distance, $\nu_{i,v}$ are the interstitial and vacancy jump frequencies, and $E^m_{i,v}$ are the interstitial and vacancy migration energies. The well-known process of radiation enhanced diffusion (RED) is due to an increase in the point defect concentrations $C_{i,v}$ above their normal thermal equilibrium values during irradiation [127]. In contrast, physical processes such as 'ionization enhanced diffusion' [2,146,147] and subthreshold elastic collisions lower the thermally-activated energy for diffusion, and are rigorously classified as radiation induced diffusion (RID) processes [167]. Therefore, the process known as 'ionization enhanced diffusion' should more correctly be called ionization induced diffusion (IID).

At this point it is not clear whether the point defect diffusion in ceramics induced by subthreshold particle irradiation is mainly due to ionization effects or subthreshold elastic collision effects. Experiments evaluating the energy dependence of electron beam stimulated regrowth of amorphous zones in irradiated semiconductors have shown that the regrowth rate increases with decreasing energy below the threshold energy for creating displacement damage [161]. Since both the elastic collision and the ionization cross-sections increase with decreasing electron energy, additional analysis such as irradiation temperature dependence or estimated magnitude of the measured cross-section is needed to discriminate between the two processes (the ionization cross-section is several orders of magnitude larger than the elastic collision cross-section). However, the experimental measurements on semiconductors suggest that the increased diffusivity is primarily associated with ionization.

There are several possible mechanisms for ionization induced diffusion [2,168]. One important mechanism (termed 'normal ionization enhanced diffusion' by Bourgoin and Corbett [168]) is based on creation of ionized point defects such as F^+ centers, which could migrate through the lattice with a lower migration energy than F centers before eventually becoming trapped or converted back to an F center. This mechanism is supported by theoretical calculations [89,92] and experimental results [169] on MgO which indicate that ionized vacancies and interstitials have a lower migration energy compared to non-ionized defects. However, it is uncertain whether an ionized point defect would generally diffuse a significant distance before reacquiring a free electron. Another intriguing ionization induced diffusion process is based on alternating F/F^+ center ionization and is known as the Bourgoin mechanism [168]. This diffusion process would produce athermal migration of point defects, and only occurs if the potential energy minimum for the ionized defect coincides with the saddle point position for the non-ionized defect and vice versa, i.e., the so-called 'bistable' configuration [147,167,168]. Experimental evidence supporting the Bourgoin mechanism has been obtained in several semiconductors [147], and it appears that this mechanism may also occur for oxygen interstitial migration in MgO [116].

Further work is needed to improve the understanding of the physical processes responsible for the observed irradiation spectrum effects in ceramics. In particular, the effect of PKA spectrum variations needs to be analyzed along with variations in the ionization/dpa ratio. It also appears that point defect diffusion in ceramics is promoted by high particle fluxes [116,162,163], but quantitative models of ionizing dose rate effects are not yet available. Finally, ionization enhanced recombination effects were not addressed in this review, but could be an important mechanism in insulators and semiconductors [165], particularly in conjunction with ionization-induced diffusion processes.

5. Conclusions

Based on our review of published experimental measurements, the threshold displacement energies for SiC, diamond and alumina (oxygen sublattice) should be revised downward from previously recommended values (cf. Table 3). Additional E_d measurements on BeO, $MgAl_2O_4$ and SiC are needed to supplement the existing data base. Furthermore, experimental E_d measurements are particularly needed for AlN and Si_3N_4, where no data currently exist.

Considerable uncertainty exists regarding the quantitative values of point defect migration enthalpies in ceram-

ics. Some of this uncertainty is likely associated with ever-present impurity trapping effects, which increase the apparent migration energy. On the other hand, radiation induced diffusion processes such as ionization induced diffusion or subthreshold elastic collisions may produce low apparent migration energies during irradiation. The available data indicate that interstitials are mobile in MgO and Al_2O_3 at temperatures well below room temperature, whereas vacancies become mobile above ~ 200°C in both materials. The significant interstitial mobility at room temperature has not been taken into account in numerous published radiation effects studies on Al_2O_3 and MgO. Further experimental radiation effects studies at liquid helium temperatures (combined with isochronal annealing) would be valuable in determining the interstitial migration energies for all ceramic materials.

Very few reliable measurements of the surviving defect fraction (displacement damage efficiency) exist for ceramics. Most of the published work was performed at room temperature, and the data analysis did not account for likely correlated and uncorrelated recombination of point defects. Therefore, the reported values are typically an underestimate of the surviving defect fraction. The limited number of cryogenic irradiation studies on MgO and Al_2O_3 suggest that the surviving defect fraction is ~ 0.3 for both materials over a wide range of PKA energies (0.1–100 keV). This apparent independence on PKA energy is in sharp contrast to work performed on light metals such as aluminum, where the surviving defect fraction (relative to the NRT calculated displacements) varies from ~ 1 to ~ 0.5 as the PKA energy increases from ~ 0.1 to ~ 50 keV. Additional experimental work is needed to evaluate the importance of correlated and uncorrelated point defect recombination effects (in conjunction with ionization induced diffusion) on the measured defect production rates in ceramics.

There is considerable evidence that the irradiation spectrum (particularly ionizing radiation) can have a pronounced effect on the microstructural evolution in ceramics and semiconductors. Recent work on MgO, Al_2O_3 and $MgAl_2O_4$ suggests that a dramatic transition in the microstructural evolution occurs at a certain ratio of the electronic to nuclear stopping power. The observed microstructure in these materials also appears to be sensitive to the magnitude of the ionizing radiation dose rate. On the other hand, ionizing radiation does not appear to have a pronounced influence on the microstructure of some ceramics such as SiC. Further work is needed to quantify the role of ionizing dose rate and PKA spectrum on the microstructural evolution of ceramics.

Acknowledgements

This work was sponsored in part by the Office of Fusion Energy Sciences, US Department of Energy under contract DE-AC05-96OR22464 with Lockheed Martin Energy Research Corp..

References

[1] N. Itoh, K. Tanimura, Radiat. Eff. 98 (1986) 269.
[2] J.C. Bourgoin, J.W. Corbett, Radiat. Eff. 36 (1978) 157.
[3] A.E. Hughes, Radiat. Eff. 97 (1986) 161.
[4] R.S. Wilks, J. Nucl. Mater. 26 (1968) 137.
[5] G.P. Pells, J. Am. Ceram. Soc. 77 (1994) 368.
[6] L.W. Hobbs, F.W. Clinard Jr., S.J. Zinkle, R.C. Ewing, J. Nucl. Mater. 216 (1994) 291.
[7] H. Matzke, Radiat. Eff. 64 (1982) 3.
[8] F.W. Clinard, Jr., L.W. Hobbs, in: Physics of Radiation Effects in Crystals, ed. R.A. Johnson and A.N. Orlov (Elsevier, Amsterdam, 1986) p. 387.
[9] L.W. Hobbs, J. Am. Ceram. Soc. 62 (1979) 267.
[10] D.R. Locker, J.M. Meese, IEEE Trans. Nucl. Sci. 19 (1972) 237.
[11] J.V. Sharp, D. Rumsby, Radiat. Eff. 17 (1973) 65.
[12] K. Urban, N. Yoshida, Philos. Mag. A44 (1981) 1193.
[13] G.P. Pells, Radiat. Eff. 64 (1982) 71.
[14] K.J. Caulfield, R. Cooper, J.F. Boas, J. Am. Ceram. Soc. 78 (1995) 1054.
[15] R.A. Youngman, L.W. Hobbs, T.E. Mitchell, J. Phys. (Paris) 41 (C6) (1980) 227.
[16] G.P. Pells, A.Y. Stathopoulos, Radiat. Eff. 74 (1983) 181.
[17] F. Agullo-Lopez, C.R.A. Catlow, P.D. Townsend, Point Defects in Materials (Academic Press, San Diego, CA, 1988).
[18] J.A. Faldowski, A.T. Motta, L.M. Howe, P.R. Okamoto, J. Appl. Phys. 80 (1996) 729.
[19] P. Agnew, Philos. Mag. A65 (1992) 355.
[20] R.S. Barnard, PhD thesis, Case Western Reserve University (1977).
[21] W.D. Compton, G.W. Arnold, Discuss. Faraday Soc. 31 (1961) 130.
[22] G. Das, J. Mater. Sci. Lett. 2 (1983) 453.
[23] G.P. Pells, D.C. Phillips, J. Nucl. Mater. 80 (1979) 207.
[24] P.D. Townsend, PhD thesis, Physics Department, University of Reading (1961).
[25] Y. Chen, D.L. Trueblood, O.E. Schow, H.T. Tohver, J. Phys. (Paris) C3 (1970) 2501.
[26] T. Sonoda, C. Kinoshita, Y. Isobe, Ann. Phys. 20 (C3) (1995) 33.
[27] G.P. Summers, G.S. White, K.H. Lee, J.H. Crawford Jr., Phys. Rev. B21 (1980) 2578.
[28] J.A. Garcia, A. Remon, J. Piqueras, Appl. Phys. A42 (1987) 297.
[29] T. Yoshiie et al., Philos. Mag. 40 (1979) 297.
[30] J. Soullard, A. Alamo, Radiat. Eff. 38 (1978) 133.
[31] D.H. Bowen, R.S. Wilks, F.J.P. Clarke, J. Nucl. Mater. 6 (1962) 148.
[32] R.S. Wilks, F.J.P. Clarke, J. Nucl. Mater. 14 (1964) 179.
[33] J.M. Cowley, Acta Crystallogr. 21 (1966) 192.
[34] J.C. Pigg, A.K. Garrison, S.B. Austermann, J. Nucl. Mater. 49 (1973) 67.
[35] B. Henderson, J.E. Wertz, Defects in the Alkaline Earth Oxides (Taylor and Francis, London, 1977).

[36] A. Bisson, J. Nucl. Mater. 10 (1963) 321.
[37] S.V. Gorbunov, A.V. Kruzhalov, M.J. Springis, Phys. Status Solidi B141 (1987) 293.
[38] I.N. Ogorodnikov, V.Y. Ivanov, A.V. Kruzhalov, Phys. Solid State 36 (1994) 1748.
[39] J.A. VanVechten, in: Materials, Properties and Preparation, Handbook on Semiconductors, Vol. 3, ed. S.P. Keller (North-Holland, New York, 1980) p. 1.
[40] T. Iwata, T. Nihara, J. Phys. Soc. Jpn. 31 (1971) 1761.
[41] R.F. Egerton, Philos. Mag. 35 (1977) 1425.
[42] G.L. Montet, G.E. Myers, Carbon 9 (1971) 179.
[43] D. Marton, K.J. Boyd, T. Lytle, J.W. Rabalais, Phys. Rev. B48 (1993) 6757.
[44] J. Koike, D.F. Pedraza, in: Proc. Int. Conf. on Beam Processing of Advanced Materials, eds. J. Singh and S.M. Copley, Mater. Res. Soc. Symp. Proc. Vol. 373 (The Mineral, Metals and Materials Society, Warrendale, PA, 1993) p. 519.
[45] H. Abe, H. Naramoto, C. Kinoshita, in: Microstructure of Irradiated Materials, eds. I.M. Robertson et al., Mater. Res. Soc. Symp. Proc. Vol. 373 (Materials Research Society, Pittsburgh, PA, 1995) p. 383.
[46] G. Lulli, A. Parisini, G. Mattei, Ultramicroscopy 60 (1995) 187.
[47] R. Smith, K. Beardmore, Thin Solid Films 272 (1996) 255.
[48] J. Koike, D.M. Parkin, T.E. Mitchell, Appl. Phys. Lett. 60 (1992) 1450.
[49] J.C. Bourgoin, B. Massarani, Phys. Rev. B14 (1976) 3690.
[50] W. Wu, S. Fahy, Phys. Rev. B49 (1994) 3030.
[51] C.D. Clark, P. Kemmey, E.W.J. Mitchell, Discuss. Faraday Soc. 31 (1961) 96.
[52] J.F. Prins, T.E. Derry, J.P.F. Sellschop, Phys. Rev. B34 (1986) 8870.
[53] I.I. Geiczy, A.A. Nesterov, L.S. Smirnov, Radiat. Eff. 9 (1971) 243.
[54] A.L. Barry, B. Lehmann, D. Fritsch, D. Bräunig, IEEE Trans. Nucl. Sci. 38 (1991) 1111.
[55] O. Chauvet et al., Mater. Sci. Forum 83–87 (1992) 1201.
[56] B. Hudson, B.E. Sheldon, J. Microsc. 97 (1972) 113.
[57] I.A. Hønstvet, R.E. Smallman, P.M. Marquis, Philos. Mag. A41 (1980) 201.
[58] P. Angelini, J.C. Sevely, K. Hasein, G. Zanchi, in: Analytical Electron Microscopy 1987, ed. D.C. Joy (San Francisco Press, San Francisco, 1987) p. 267.
[59] D. Volm, B.K. Meyer, E.N. Mokhov, P.G. Baranov, in: Diamond, SiC and Nitride Wide Bandgap Semiconductors, eds. C.H. Carter Jr. et al., Mater. Res. Soc. Symp. Proc., Vol. 339 (Materials Research Society, Pittsburgh, PA, 1994) p. 705.
[60] J. Wong et al., J. Nucl. Mater. 212–215 (1994) 143.
[61] B.T. Kelly, Physics of Graphite (Applied Science, Englewood, NJ, 1981).
[62] B. Massarani, J.C. Bourgoin, Phys. Rev. B14 (1976) 3682.
[63] I.T. Flint, J.N. Lomer, Physica B116 (1983) 183.
[64] J. Koike, T.E. Mitchell, D.M. Parkin, Appl. Phys. Lett. 59 (1991) 2515.
[65] H.C. Huang, N.M. Ghoniem, J.K. Wong, M.I. Baskes, Modelling Simul. Mater. Sci. Eng. 3 (1995) 615.
[66] A. El-Azab, N.M. Ghoniem, J. Nucl. Mater. 191–194 (1992) 1110.
[67] L.W. Hobbs, in: Introduction to Analytical Electron Microscopy, eds. J.J. Hren, J.I. Goldstein and D.C. Joy (Plenum, New York, 1979) p. 437.
[68] J.A. VanVechten, in: Radiation Effects in Semiconductors, eds. N.B. Urli and J.W. Corbett, IOP Conf. Ser. 31 (Institute of Physics, London, 1977) p. 441.
[69] D.L. Medlin, L.E. Thomas, D.G. Howitt, Ultramicroscopy 29 (1989) 228.
[70] M.J. Norgett, M.T. Robinson, I.M. Torrens, Nucl. Eng. Des. 33 (1975) 50.
[71] Y. Matsutani, S. Ishino, J. Appl. Phys. 48 (1977) 1822.
[72] K.B. Winterbon, Nucl. Sci. Eng. 53 (1974) 261.
[73] N. Andersen, P. Sigmund, K. Dan. Vidensk. Selsk. Mat.-Fys. Medd. 39 (1974).
[74] K. Winterbon, P. Sigmund, J. Sanders, K. Dan. Vidensk. Selsk. Mat.-Fys. Medd. 37 (1970).
[75] J.A. Dennis, Radiat. Eff. 8 (1971) 87.
[76] D.M. Parkin, C.A. Coulter, J. Nucl. Mater. 101 (1981) 261.
[77] D.M. Parkin, C.A. Coulter, J. Nucl. Mater. 103&104 (1981) 1315.
[78] C.A. Coulter, D.M. Parkin, J. Nucl. Mater. 88 (1980) 249.
[79] H. Huang, N.M. Ghoniem, J. Nucl. Mater. 199 (1993) 221.
[80] G.F. Dell, A.N. Goland, J. Nucl. Mater. 102 (1981) 246.
[81] D.M. Parkin, C.A. Coulter, J. Nucl. Mater. 85&86 (1979) 611.
[82] D.M. Parkin, Nucl. Instrum. Meth. B46 (1990) 26.
[83] E. Iguchi, K. Otake, T. Yamamoto, H. Nishikawa, J. Nucl. Mater. 169 (1989) 55.
[84] N.M. Ghoniem, S.P. Chou, J. Nucl. Mater. 155–157 (1988) 1263.
[85] C. Kinoshita, K. Hiyashi, T.E. Mitchell, in: Structure and Properties of MgO and Al_2O_3 Ceramics, ed. W.D. Kingery, Advances in Ceramics, Vol. 10 (American Ceramic Society, Columbus, OH, 1984) p. 490.
[86] W.C. Mackrodt, in: Structure and Properties of MgO and Al_2O_3 Ceramics, ed. W.D. Kingery, Advances in Ceramics, Vol. 10 (American Ceramic Society, Columbus, OH, 1984) p. 62.
[87] B. Henderson, D.H. Bowen, A. Briggs, R.D. King, J. Phys. (Paris) C4 (1971) 1496.
[88] M.J.L. Sangster, D.K. Rowell, Philos. Mag. A44 (1981) 613.
[89] E.A. Kotomin, M.M. Kuklja, R.I. Eglitis, A.I. Popov, Mater. Sci. Eng. B37 (1996) 212.
[90] Y. Chen, J.L. Kolopus, W.A. Sibley, Phys. Rev. 182 (1969) 960.
[91] C. Scholz, P. Ehrhart, in: Beam Solid Interactions: Fundamentals and Applications, eds. M. Nastasi et al., Mater. Res. Soc. Symp. Proc. Vol. 279 (Materials Research Society, Pittsburgh, PA, 1993) p. 427.
[92] T. Brudevoll, E.A. Kotomin, N.E. Christensen, Phys. Rev. B53 (1996) 7731.
[93] W.D. Kingery, J. Nucl. Mater. 24 (1967) 21.
[94] A.I. VanSambeek, R.S. Averback, C.P. Flynn, M.H. Yang, in: Microstructure of Irradiated Materials, eds. I.M. Robertson et al., Mater. Res. Soc. Symp. Proc. Vol. 373 (Materials Research Society, Pittsburgh, PA, 1995) p. 293.
[95] G.J. Dienes, A.C. Damask, J. Appl. Phys. 29 (1958) 1713.
[96] W.A. Sibley, Y. Chen, Phys. Rev. 160 (1967) 712.
[97] G. Rius, R.T. Cox, Phys. Lett. A27 (1968) 76.

[98] G. Rius, R.T. Cox, P. Freund, J. Owen, J. Phys. (Paris) C7 (1974) 581.
[99] A.E. Hughes, J. Phys. (Paris) 34 (C9) (1973) 515.
[100] Y.M. Annenkov, A.M. Pritulov, Sov. Phys. Solid State 23 (1981) 616.
[101] T. Sonoda, C. Kinoshita, A. Manabe, J. Nucl. Mater. (1997), in press.
[102] Y. Oishi, K. Ando, N. Suga, W.D. Kingery, J. Am. Ceram. Soc. 66 (1983) C130.
[103] K.P.D. Lagerlof, T.E. Mitchell, A.H. Heuer, J. Am. Ceram. Soc. 72 (1989) 2159.
[104] P.W.M. Jacobs, E.A. Kotomin, Philos. Mag. A68 (1993) 695.
[105] K. Atobe, N. Nishimoto, M. Nakagawa, Phys. Status Solidi A89 (1985) 155.
[106] B. Lesage, A.M. Huntz, G. Petot-ervas, Radiat. Eff. 75 (1983) 283.
[107] H.-E. Schaefer, M. Forster, Mater. Sci. Eng.A 109 (1989) 161.
[108] A.E. Palladino, W.D. Kingery, J. Chem. Phys. 37 (1962) 957.
[109] J.M. Bunch, F.W. Clinard Jr., J. Am. Ceram. Soc. 57 (1974) 279.
[110] B. Jeffries, G.P. Summers, J.H. Crawford Jr., J. Appl. Phys. 51 (1980) 3984.
[111] K. Atobe, M. Nakagawa, Cryst. Latt. Def. Amorph. Mater. 17 (1987) 229.
[112] G.P. Pells, AERE Harwell Report AERE-R9359 (1979).
[113] B. Jeffries, J.D. Brewer, G.P. Summers, Phys. Rev. B24 (1981) 6074.
[114] R.T. Cox, Phys. Lett. 21 (1966) 503.
[115] I.K. Abdukadyrova, Sov. At. Energy 62 (1987) 221.
[116] S.J. Zinkle, in: Microstructure Evolution During Irradiation, eds. I.M. Robertson et al., Mater. Res. Soc. Symp. Proc., Vol. 439 (Materials Research Society, Pittsburgh, PA, 1997) p. 667.
[117] G.W. Arnold, W.D. Compton, Phys. Rev. Lett. 4 (1960) 66.
[118] C.D. Clark, E.W.J. Mitchell, in: Radiation Effects in Semiconductors, eds. N.B. Urli and J.W. Corbett, Institute of Physics Conf., Vol. 31 (Institute of Physics, London, 1977) p. 45.
[119] A.D. Mokrushin, A.I. Girka, A.V. Shishkin, Phys. Status Solidi A128 (1991) 31.
[120] H. Itoh et al., J. Appl. Phys. 77 (1995) 837.
[121] A.A. Rempel, H.-E. Schaefer, Appl. Phys. A61 (1995) 51.
[122] L.A. de Sousa Balona, J.H.N. Loubser, J. Phys. (Paris) C3 (1970) 2344.
[123] L.L. Snead, S.J. Zinkle, in: Microstructure Evolution During Irradiation, ed. I.M. Robertson et al., Mater. Res. Soc. Symp. Proc., Vol. 439 (Materials Research Society, Pittsburgh, PA, 1997) p. 595.
[124] R.S. Averback et al., J. Nucl. Mater. 113 (1983) 211.
[125] S.J. Zinkle, B.N. Singh, J. Nucl. Mater. 199 (1993) 173.
[126] S.J. Zinkle, J. Nucl. Mater. 150 (1985) 140.
[127] R. Sizmann, J. Nucl. Mater. 69&70 (1978) 386.
[128] V.A. Borodin, A.I. Ryazanov, D.G. Sherstennikov, J. Nucl. Mater. 202 (1993) 169.
[129] L.K. Mansur, J. Nucl. Mater. 206 (1993) 306.
[130] B.D. Evans, J. Comas, P.R. Malmberg, Phys. Rev. B6 (1972) 2453.
[131] M. Okada, T. Seiyama, C. Ichihara, M. Nakagawa, J. Nucl. Mater. 133&134 (1985) 745.
[132] B. Henderson, D.H. Bowen, J. Phys. (Paris) C4 (1971) 1487.
[133] Y. Chen et al., in: Radiation Effects and Tritium Technology for Fusion Reactors, Gatlinburg, TN, Vol. II, eds. J.S. Watson and F.W. Wiffen (USERDA, 1975) p. 492.
[134] R.S. Averback, P. Ehrhart, A.I. Popov, A.v. Sambeek, Radiat. Eff. Def. Solids 136 (1995) 169.
[135] P. Agnew, Nucl. Instrum. Meth. B65 (1992) 305.
[136] B.D. Evans, in: Ion Implantation in Semiconductors, ed. S. Namba (Plenum, New York, 1975) p. 511.
[137] J. Valbis, N. Itoh, Radiat. Eff. Def. Solids 116 (1991) 171.
[138] S.D. Berger et al., Philos. Mag. B55 (1987) 341.
[139] J.E. Bonevitch, L.D. Marks, Ultramicroscopy 35 (1991) 161.
[140] S.D. Berger, J.M. Macaulay, L.M. Brown, Philos. Mag. Lett. 56 (1987) 179.
[141] M.R. McCartney, D.J. Smith, Surf. Sci. 35 (1991) 169.
[142] Y. Katano et al., J. Nucl. Mater. 212–215 (1994) 1039.
[143] M.L. Knotek, P.J. Feibelman, Surf. Sci. 90 (1979) 78.
[144] M.L. Knotek, Rep. Prog. Phys. 47 (1984) 1499.
[145] A.L. Shluger, J. Phys.: Condens. Matter 3 (1991) 8027.
[146] J.W. Corbett, J.C. Bourgoin, IEEE Trans. Nucl. Sci. 18 (1971) 11.
[147] J.C. Bourgoin, Radiat. Eff. Def. Solids 111–112 (1989) 29.
[148] D.G. Walker, J. Nucl. Mater. 14 (1964) 195.
[149] G.W. Arnold, G.B. Krefft, C.B. Norris, Appl. Phys. Lett. 25 (1974) 540.
[150] G.B. Krefft, J. Vac. Sci. Technol. 14 (1977) 533.
[151] G.B. Krefft, E.P. EerNisse, J. Appl. Phys. 49 (1978) 2725.
[152] R. Brenier et al., Nucl. Instrum. Meth. B80&81 (1993) 1210.
[153] S.J. Zinkle, S. Kojima, J. Nucl. Mater. 179–181 (1991) 395.
[154] Y. Chen, M.M. Abraham, H.T. Tohver, Phys. Rev. Lett. 37 (1976) 1757.
[155] Y. Chen, R. Gonzalez, K.L. Tsang, Phys. Rev. Lett. 53 (1984) 1077.
[156] D.A. Thompson, R.G. Macauley-Newcombe, Canadian Fusion Fuels Technology Project, Mississauga, Ont., Canada Report CFFTP G-9586 (1996).
[157] S.J. Zinkle, L.L. Snead, Nucl. Instrum. Meth. B116 (1996) 92.
[158] L.M. Wang et al., in: Microstructure Evolution During Irradiation, eds. I.M. Robertson et al., Mater. Res. Soc. Symp. Proc., Vol. 439 (Materials Research Society, Pittsburgh, PA, 1997) p. 583.
[159] H. Abe, C. Kinoshita, Y. Denda, in: Microstructure of Irradiated Materials, eds. I.M. Robertson et al., Mater. Res. Soc. Symp. Proc., Vol. 373 (Materials Research Society, Pittsburgh, PA, 1995) p. 487.
[160] A. Meldrum, L.A. Boatner, R.C. Ewing, J. Mater. Res. 12 (1997) 1816.
[161] I. Jencic, I.M. Robertson, J. Mater. Res. 11 (1996) 2152.
[162] S.J. Zinkle, Nucl. Instrum. Meth. B91 (1994) 234.

[163] S.J. Zinkle, J. Nucl. Mater. 219 (1995) 113.
[164] S.J. Zinkle, in: Microstructure of Irradiated Materials, eds. I.M. Robertson et al., Mater. Res. Symp. Symp. Proc., Vol. 373 (Materials Research Society, Pittsburgh, PA, 1995) p. 287.
[165] L.C. Kimerling, Solid-State Electron. 21 (1978) 1391.
[166] K. Yasuda, C. Kinoshita, R. Morisaki, H. Abe, H. Naramoto, in: Proc. 7th Int. Symp. on Advanced Nuclear Energy Research (1997) p. 384; K. Yasuda, C. Kinoshita, R. Morisaki, H. Abe, Philos. Mag. A (1997) in press.
[167] U. Gösele, W. Frank, A. Seeger, in: Defects and Radiation Effects in Semiconductors 1978, ed. J.H. Albany, IOP Conf. Ser. 46 (Institute of Physics, London, 1979) p. 538.
[168] J.C. Bourgoin, J.W. Corbett, J. Chem. Phys. 59 (1973) 4042.
[169] S. Clement, E.R. Hodgson, Phys. Rev. B36 (1987) 3359.